3.1 THE BTEM SILICON-STRIP TRACKER CONVERTER

The proposed GLAST LAT Silicon-Strip Tracker Converter is composed of 16 modules, each with 18 *x,y* planes of detectors. The BTEM tracker implements a slightly smaller module built according to an earlier LAT design with a 5×5 array of tower modules and only 16 *x,y* planes (Hernando, 1999).

3.1.1 Goals of the Tracker ATD Program and the BTEM

The principal objective of Option 1 of the Tracker ATD program was to construct a full-scale engineering model of a single GLAST tracker module and operate it in a beam test together with the other BTEM subsystems. The most important goals of this exercise are the following:

- Demonstrate operation of our custom low-noise, low-power readout electronics in a system environment, achieving the required noise occupancy of less than 10^{-4} with 99% or greater efficiency.
- Demonstrate front-end data acquisition electronics capable of sustained high trigger rates (10 kHz) with low dead time (<1%) and with sufficient redundancy to minimize risk of single-point system failures.
- Demonstrate a low-mass, high-precision support structure that can survive a Delta-II launch.
- Develop assembly and QC techniques that can lead to timely construction of the GLAST Tracker with <1% dead channels.
- Demonstrate adequate cooling and thermal control in a vacuum.

3.1.2 Deliverables for Option 1

We proposed the following deliverables for Option 1, all of which have been achieved, except for analysis of the data, which is in progress:

- Make a complete, detailed engineering design of the tracker module. This was accomplished for the BTEM Tracker, and the engineering drawings are archived at SLAC. The proposed LAT flight Tracker will differ in a number of details, based on changes in overall dimensions and on information learned during the ATD program.
- Update the existing Monte Carlo model to finalize the instrument performance. This was accomplished, and the model was extensively used in preparation of our proposal for the GLAST LAT. In addition, we made extensive progress on improvements to the event reconstruction code and algorithms, such as implementation of a Kalman-filter fit and new, more sophisticated pattern recognition code. All of this is part of the GLASTSIM program.
- Construct a complete Tracker module. This was accomplished, and the module was delivered to SLAC in November 1999.
- Integrate the Tracker module with the BTEM Calorimeter, ACD, and DAQ and operate in the SLAC test beams. This was completed during December 1999 and January 2000, and the data are archived at SLAC.
- Assess the BTEM performance as a gamma-ray telescope and verify the Monte Carlo simulations. This work is in progress through analysis of the beam-test data. Some preliminary results are included here, and the final results will be published.

3.1.3 Silicon-Strip Detectors

The BTEM silicon-strip detectors are 400 μm thick and have a strip pitch of 194 μm. The detectors have an *n*-intrinsic substrate, and the *p*-type strip implants are AC coupled to metal strips of width 52 μm and biased via ≈60 MΩ polysilicon resistors. 547 tested detectors were purchased from Hamamatsu Photonics, 296 of size 6.4×6.4 cm^2 and 251 of size 6.4×10.7 cm^2. Of those, 250 of the small size were used in the BTEM in the form of 5-detector-long "ladders", while 237 of the larger size were used as 3-detector-long ladders. One additional ladder was constructed of detectors of the larger size obtained from Micron Semiconductor, to make a total of 130 ladders all of the same 32-cm length. This is 81% of the number

of ladders needed to populate all of the 16 *x,y* planes. (6 more ladders were used in early prototype assemblies and a few detectors were used for qualification studies.) Table 3.1.1 shows how the ladders are distributed in the BTEM tracker module.

The manufacturers tested the detectors for acceptable leakage current and defective strips. We visually scanned them and checked again their leakage current before using. Only 9 detectors were rejected by this procedure.

3.1.4 Detector Ladder Assembly

Detectors were assembled into ladders by edge bonding with epoxy, as illustrated in Figure 3.1.1. One detector edge was dipped in a thin film of epoxy, placed on a simple jig, and butted against the next detector. After curing, an automated optical measuring machine checked the relative alignment. The detectors were supported and aligned on the jig by plastic posts, which were designed for the small detectors. They did not support the long detectors optimally, resulting in larger vertical steps (by as much as 50 μm) between detectors. This manual assembly procedure resulted in a typical bond thickness of about 30 μm and rms deviations between strips from one detector to the next of 15 μm in the plane of the ladder.

After edge bonding, the ladders were placed in custom-designed work-storage fixtures and transferred to UCSC, where the leakage current of the detectors was again checked. Then the wire bonds were made from detector to detector, followed by another check of the leakage current. In addition, the AC pad of each strip was probed, in an automated probe station, to measure the capacitance to the substrate. The results of this measurement were used to detect strips with broken capacitors, shorts, missing wire bonds, or open metal. The rate of wire-bonding failures necessitating repairs was only 0.06% overall, or 0.04% after removing from the statistics a few ladders that were known to have been bonded with a worn-out wedge or badly calibrated machine.

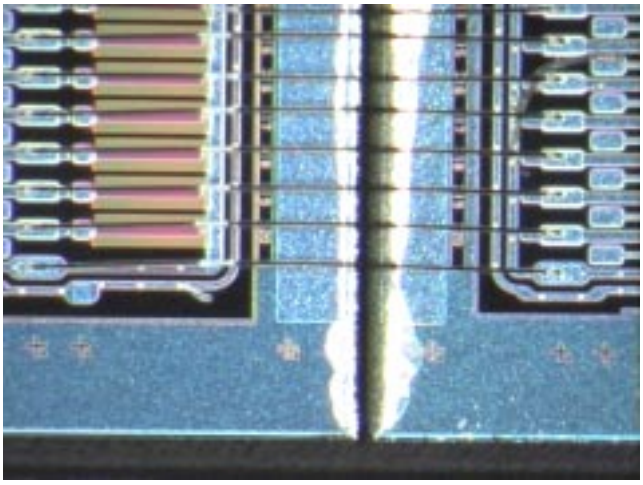

Figure 3.1.1. Detail of the edge bond between two detectors in a ladder. Wire bonds are also visible (before encapsulation).

Table 3.1.1. Configuration of the converters and detector ladders in the BTEM tracker.

Layer	Tray	Detector Size	Converter	# Ladders	Number of Detectors
16 y	17	small	3.5%	3	15
16 x	16	small		3	15
15 x	16	small	3.5%	3	15
15 y	15	mixed		3	10S + 3L
14 y	15	small	3.5%	3	15
14 x	14	small		3	15
13 x	14	small	3.5%	3	15
13 y	13	small		3	15
12 y	13	small	3.5%	3	15
12 x	12	small		3	15
11x	12	small	3.5%	3	15
11 y	11	small		3	15
10 y	11	small	3.5%	3	15
10 x	10	small		3	15
9 x	10	small	3.5%	4	20
9 y	9	large		4	12
8 y	9	small	3.5%	5	25
8 x	8	large		5	15
7 x	8	large	3.5%	5	15
7 y	7	large		5	15
6 y	7	large	3.5%	5	15
6 x	6	large		5	15
5 x	6	large	25%	5	15
5 y	5	large		5	15
4 y	5	large	25%	5	15
4 x	4	large		5	15
3 x	4	large	25%	5	15
3 y	3	large		5	15
2 y	3	large	None	5	15
2 x	2	large		5	15
1 x	2	large	None	5	15
1 y	1	large		5	15

The ladders were then moved to a potting fixture, which was a vacuum jig that supported the ladders at all points except directly under the adhesive joints. A mask fit onto the jig and over the ladder, leaving exposed only a slit above the wire bonds. Epoxy was sprayed through the mask to fill completely the wire bonds without covering the remainder of the detectors. This procedure worked well but was time consuming, as it relied too much on manual/visual control. A final check of the leakage current was done before mounting onto the tray.

Detectors with known defective strips (from testing at the manufacturer) were placed at the ends of ladders furthest from the amplifiers. Some additional defective strips were detected by our testing after wire bonding. In all cases, the wire bonds connecting to the defective strips were removed. As a result, 18 out of 41,600 strips (0.04%) in the BTEM are effectively shorter than 32-cm by at least one detector length. 10 of those defects are due to shorted AC coupling capacitors, 6 are due to internal shorts in the aluminum strips, and 2 are due to internal breaks in the aluminum strips. Four ladders were discarded during construction, two because they developed high leakage current and two because of errors made in assembly.

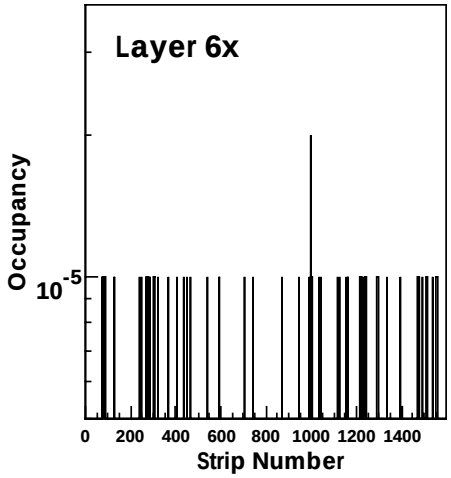

Figure 3.1.2. Noise occupancy measured for 1600 channels of one layer of the BTEM Tracker. The number of hits in 100,000 random triggers is plotted for each strip. The average occupancy is clearly well below 10^{-5}.

Since building ladders will be one of the major undertakings of the LAT Tracker construction, this experience is extremely valuable. It demonstrates that a very low rate of defective or damaged strips can be readily achieved, but it also shows us exactly where work needs to be put into developing the assembly-line procedures for the LAT construction.

3.1.5 Converter Foils

Lead foils are used as a converter material in the BTEM Tracker, each cut to match the active area of the silicon-strip sensor immediately below. The Tracker is composed of two measurement sections, Front and Back. The Front consists of 11 *x*,*y* planes with 3.5% radiation-length foils, while the Back consists of 3 *x*,*y* planes of 25% foils (see Table 3.1.1). Finally, at the bottom there are two *x*,*y* planes with no converter foils. This configuration is a close approximation to what we have proposed for the LAT flight instrument and will be used to validate the simulations upon which that design was based.

3.1.6 Tracker Readout Electronics

The readout electronics for the BTEM Tracker were designed to be as close as possible to what we believe is needed for the LAT flight instrument. The low-power, low-noise amplifier-discriminator design (Johnson, 1998) was already proven in the GLAST 1997 beam test (Atwood, 1999). In the BTEM, however, we have also implemented the complete design for the data-acquisition aspects of the front-end electronics.

3.1.6.1 Requirements

The prototype electronics for the BTEM Tracker front-end readout meet the following requirements when integrated with 32-cm long detector ladders:

- Noise occupancy of less than 10^{-4} with 99% or greater efficiency. See Figure 3.1.2, Figure 3.1.3, and Figure 3.1.11.
- Triggering: self-triggering of the BTEM tracker was successfully demonstrated in the

beam test (although most beam-test data were taken using a trigger from the accelerator). The noise trigger rate was negligible (8 to 10 Hz).

- Low power: 210 μW/channel has been achieved in the BTEM electronics, including all digital activity on the front-end readout board, assuming a high (12 kHz) trigger rate.
- Compactness: all of the front-end electronics for a detector layer fit on the side of a Tracker tray. See Figure 3.1.8.
- Redundancy: each amplifier-discriminator chip can be read out by either of two paths, so at least two failures would have to occur before the system would lose more than 64 channels.
- Readout speed and dead time: in principle the Tracker readout can operate with only a few microsecond dead time per event, but in practice the dead time is established by the Calorimeter readout. Simulations of on-orbit background predict an average Tracker readout time for background events of only 7.3 μs, with a maximum of 203 μs. Since the front-end electronics include an 8-event FIFO buffer, with the amplifier kept alive during readout, the tracker can read out well in excess of 10 kHz with negligible dead time. In fact, the buffer occupancy never exceeded 6 in the simulations, so the Tracker *never* increased the dead time with respect to that imposed by the Calorimeter.

3.1.6.2 Hybrids (Multi-Chip Modules)

Each layer of silicon-strip detectors is read out by a single hybrid, which consists of 27 VLSI chips mounted directly onto a printed circuit board. Figure 3.1.4 shows a photograph of part of one hybrid. Five 64-channel amplifier-discriminator chips (GTFE64) are lined up along the top with their inputs wire bonded to the Kapton circuit that carries the signals around the tray corner from the detectors (see Section 3.1.6.4). A fifth chip is visible near the connector. It is one of two redundant readout controllers (GTRC), the other one being located at the other end of the hybrid. The passive surface-mount components consist of power

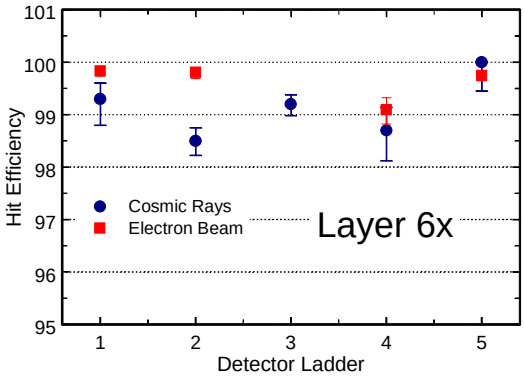

Figure 3.1.3. Measurements of the average MIP efficiency per detector ladder in one layer of the BTEM tracker, using the same discriminator thresholds as used for the occupancy results in Figure 3.1.2. The cosmic rays were incident over a continuous range of angles and positions, while the 20 GeV electron beam was scanned across 4 *x* positions (times 4 *y* positions) at normal incidence and was ≈1 cm wide (see also Figure 3.1.11). Inefficiency due to dead areas between detectors is excluded by this analysis, but some apparent inefficiency is due to errors in track reconstruction, especially for cosmic rays.

supply filters, fuses, decoupling capacitors, termination resistors, resistors to set the amplifier bias currents, and a thermistor for temperature monitoring.

During readout, data latched within the GTFE64 buffers are shifted down the line of chips and into the GTRC chip, where they are formatted into a list of addresses of hit strips and then sent to the DAQ. Figure 3.1.5 illustrates the flow of data and control signals in this system, showing in particular how redundancy is implemented in order to avoid catastrophic single-point failures. Not shown in the figure

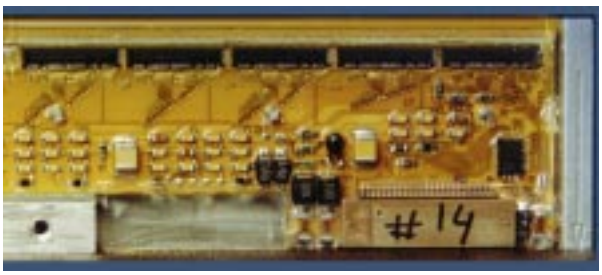

Figure 3.1.4. Photograph of the right-most 1/5 of a hybrid, shown mounted on the side of a BTEM tray.

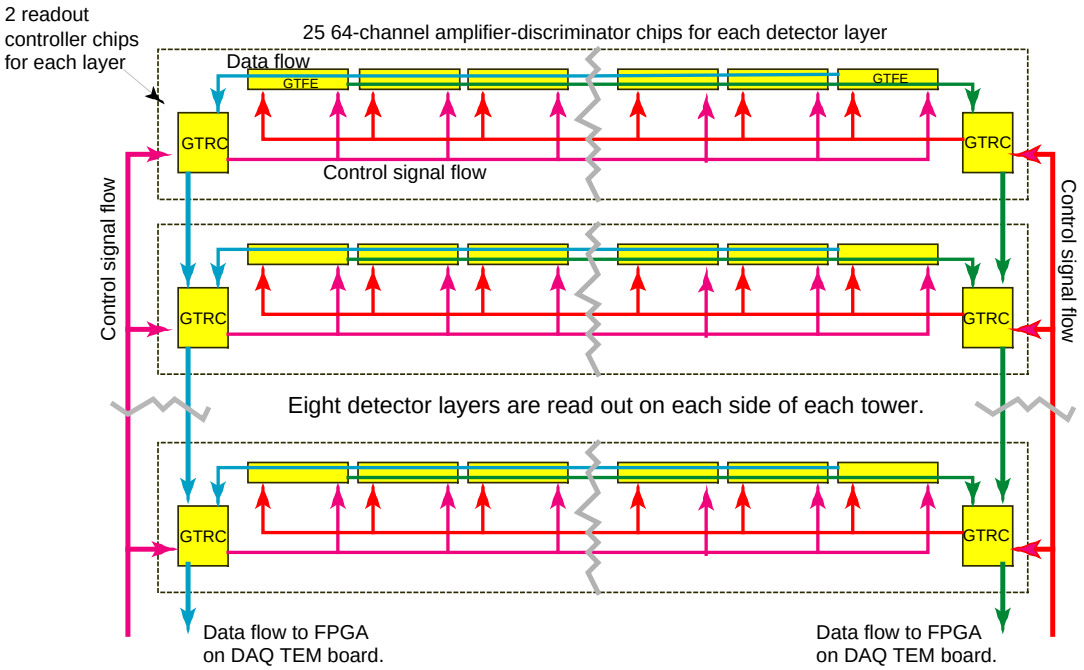

Figure 3.1.5. The readout scheme of the BTEM Tracker front-end electronics, which implements the complete functionality planned for the flight system. Each readout chip can send its data to the DAQ by either of two redundant paths indicated by blue and green arrows. Similarly, each chip can be controlled by either of two paths, indicated by red and magenta arrows.

are the "Fast-OR" signals sent to the DAQ and used to generate triggers. Each Fast-OR is simply the logical OR of all (unmasked) discriminator outputs for a single Tracker layer.

The boards are 8-layer FR4-based printed circuits with a gold body for wire bonding. The high number of layers is needed in order to implement a careful design for isolation of digital noise from the analog power and ground and to ensure a clean, low-noise flow of the small signal currents through the amplifiers and, via capacitors, back to the detector bias plane. The boards were loaded with passive components and connectors by a commercial vendor followed by testing at UCSC before being loaded by the same vendor with chips and wire bonded. Testing and burn-in, for one week, of the completed modules was then done at UCSC. After mounting onto a tray and wire bonding to the flex circuit, each module was fully encapsulated in a soft space-qualified silicone.

Some problems were found with the hybrids that can easily be avoided in the future. First of all, some solder bridges were found that were due to improper spacing of a few of the surface-mount parts. Second, there were some problems of shorting of traces to the backs of the chips and mechanical damage of some traces near the hybrid ends. Those problems can be avoided by coating the board with a solder mask, leaving open only the chip wire-bond points as well as the solder pads.

3.1.6.3 ASICs

Two ASICs were custom designed for the Tracker readout. They implement the full functionality desired for the flight instrument and satisfy the requirements on noise performance and power consumption as well as data rate. They were implemented in the HP 0.8 µm CMOS process, but they have not been space qualified.

In addition to amplifiers and discriminators for each of the 64 channels, the GTFE64 readout chip includes trigger logic, a calibration system, buffering for 8 events, dual redundant control and configuration via serial commands, DACs for setting the threshold and calibration ampli-

tudes, and LVDS input-output. Its layout is shown in Figure 3.1.7. The chip includes three 64-channel programmable mask registers: one to select channels for calibration pulsing, one to remove noisy channels from the Fast-OR trigger signal, and one to remove noisy channels from the data stream.

The readout chips do not interact directly with the DAQ. Rather, all communication takes place via the GTRC readout controller chips over LVDS links. In addition to buffering clock, trigger, and command signals, the GTRC chips control the readout sequence, format the data into packets of addresses of hit strips, buffer the data, and handle the readout protocol with the DAQ. The chip also calculates the time-over-threshold of the Fast-OR signal and includes it in the data stream. Figure 3.1.6 shows the layout of the GTRC chip.

The ASICs were acquired through MOSIS and then tested at UCSC on an automated probe station before dicing the wafers.

3.1.6.4 Bias Circuits and Kapton Cables

The 5 detector ladders of a tray are mounted on a Kapton circuit that covers the entire tray surface. The circuit carries the bias current (at about 100V) from the hybrid to 1-cm^2 pads onto which the detectors are bonded with a conductive epoxy. A hatched ground plane lies below the bias circuitry, to shield the detectors from possible noise in the mechanical structure. A narrow tongue extends from one edge, bends around the tray corner, and is bonded to the hybrid. This tongue contains 1600 narrow strips, with gold body, that are bonded on one end to the detector AC pads and on the other end to the amplifier inputs of the GTFE64 chips. It also contains additional wider strips for the bias current and ground return.

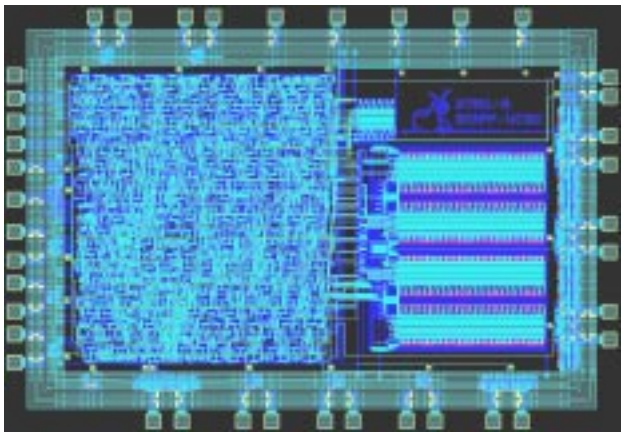

Figure 3.1.6. Layout of the GTRC readout controller chip. Control logic is on the left, while the data buffers and time-over-threshold FIFO are on the right.

Eight custom 4-layer Kapton flex circuit cables connect the hybrids to the repeater boards and, ultimately, the DAQ. Two are visible in Figure 3.1.12. Two layers are essentially used for power and ground, both digital and analog, while the other two layers hold the differential-pair traces used for digital signals. Side arms bring the signals and power to individual hybrids via 25-pin Nanonics connectors, while a 37-pin Nanonics connector mates with the repeater card. The connectors are bonded to the cable and soldered to surface-mount pads. A few resistors are also soldered to the cable near the upper end to provide termination for digital signals.

3.1.6.5 Repeater Boards and Twist-Pair Cables

In the LAT flight-instrument design, the tower electronics modules (TEM) are mounted just under the calorimeter, so the Kapton cables will be made long enough to reach that point. In the BTEM, however, the DAQ electronics were mounted in a VME crate. Therefore, the Kapton cables were each connected to a small PC board

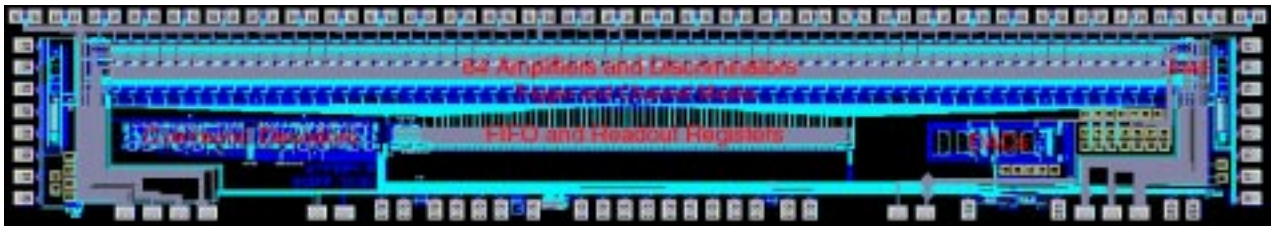

Figure 3.1.7. Layout of the GTFE64 front-end readout chip.

(repeater card), which in turn connected to a 2 m Glenair shielded twist-pair cable with Micro-D connectors on each end. To be safe, onto this board we placed a set of LVDS chips to boost the signals traveling from the GTRC chips to the DAQ, since the GTRC chips were not designed to send signals down long transmission lines with 100 Ω termination. The boards also include ferrite cores, to block possible digital noise from coming up the cables from VME, and relatively large filtering capacitors for the power.

Furthermore, the repeater cards connect the analog and digital grounds together and connect them to the shield composed of the tracker base and walls (analog and digital power are separate all the way back to the power supplies). Care was taken not to connect the shield to anything else, such as the calorimeter or beam-test support structure. It is connected to the VME crate via the shields of the Glenair cables. In this way the amplifier grounds are ultimately referenced to this shield—overall movement of the shield with respect to the surroundings has no effect on the signals seen by the amplifiers. In fact, there was no evidence of any pickup of noise by the Tracker front-end electronics during the beam-test running.

3.1.7 Tracker Trays

3.1.7.1 Mechanical Design

The tray mechanical design is based upon a composite panel, composed of a machined aluminum closeout, aluminum hex-cell core, and carbon fiber face sheets. As shown in Figure 3.1.9, the lead converter foils, Kapton bias circuits, and silicon-strip detectors are bonded to the faces of the panel, while the readout electronics are mounted onto the sides with screws.

The cores are 25 μm thick aluminum with 1-cm cell size. The face sheets are about 75 μm thick and made from a single-layer woven fabric of carbon fibers impregnated with epoxy. The converter foils are individual rectangles of lead, each cut to the size of the active region of the single detector mounted over the foil. The goal is to keep converter material out of the dead

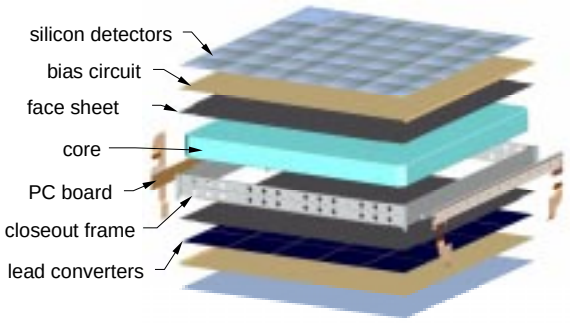

Figure 3.1.9. Description of the tray composite structure.

regions between detectors, to minimize the number of non-optimal conversions. This does not quite work in the *x,y* planes that are composed of long detectors, since in those planes the foils can match only the *x* or *y* detectors, but not both. In the flight design all detectors will be square, to avoid this problem.

The corners of the tray are machined into posts with precision holes drilled through the center, which establish reference points for a alignment of detectors onto the trays and for alignment of one tray to the next. Hollow pins inserted into the holes fix the tray-to-tray alignment. Vectran cables tensioned to about 110 Newtons pass through the corner-post holes from the bottom of the module to the top, to hold the assembly in alignment while mounting the readout cables and exterior walls.

The corner posts and other bosses on the closeouts have tapped holes for mounting of the 1.5 mm thick aluminum exterior walls. Heat from the electronics flows through the closeout

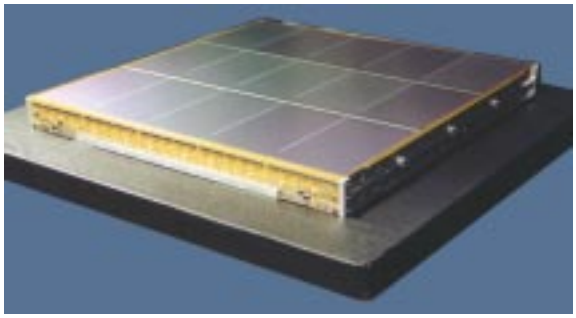

Figure 3.1.8. Photograph of one of 17 trays of the BTEM Tracker. 1600 strips in the silicon detectors on the top surface are read out by the electronics on the front edge. Not visible are a full plane of detectors on the bottom of the tray and the associated readout electronics on the rear edge.

boss located just below the PC board and into the wall.

3.1.7.2 Assembly

The tray panel structures were assembled at SLAC. The closeout was held flat and square in a jig while the core and face sheets were bonded and clamped. The lead foils and Kapton bias circuits were also bonded in the same fixture. Aluminum rails were attached by screws to the two non-electronics sides of the trays and served to support the tray during further assembly work. The remaining 4 sides of the tray were then covered by acrylic panels, each of which could be individually removed for access.

The hybrid circuits were bonded to the tongue of the Kapton bias circuit at UCSC, using a precision fixture that attached to the tray and supported the circuit in the plane of the face sheet. This was a delicate procedure, since squeeze-out and coverage of the adhesive had to be carefully controlled all along the narrow bonding region, and the alignment had to be very precise to ensure that the screw holes in the hybrid would match those in the closeout after bending the hybrid down. Furthermore, after this step there is no possibility of removing the hybrid from the tray in order to replace it or repair it. For those reasons, we intend to modify substantially and improve this aspect of the design for the LAT flight instrument.

Finally, the detector ladders were aligned to the tray and bonded to the kapton bias circuit using conductive epoxy, followed by wire bonding to the narrow traces on the tongue of the bias circuit. 50 μm thick tape was used as a spacer to control the thickness of the adhesive bond and maintain the detector *z* alignment. A small amount of epoxy was also used to support the detectors along the edge where wire bonding was done. Wire bonding to the Kapton was more difficult than the wire bonding within the detector ladders, with a failure rate of about 0.2% (failures are always repaired, but the extra work is time consuming).

The trays were optically surveyed after assembly. The maximum deviations in ladder placement were 55 μm, resulting in maximum ladder rotations of about 0.01°.

3.1.7.3 Tray Vibration Test.

Vibration testing was carried out at GSFC on the first tray to be instrumented with a complete layer of operational detector ladders and readout electronics. The setup is shown in Figure 3.1.10. The tray was supported on the corner posts and by thin plates along the side (to simulate tower walls).

The tray fundamental frequency was measured to be 700 Hz (drum mode) with a Q of about 35, compared with our numerical model, which predicted a frequency of 654 Hz. The tray was also subjected to a 14g rms random vibration test (full GEVS qualification levels), which it survived with no damage, including no loss of any of the wire bonds. The detector leakage current in all ladders was unchanged by the vibration testing.

3.1.8 Quality Control

Assembly of the ladders and trays was carefully tracked by use of a Filemaker-Pro database. Paper travelers were kept with each item and used to sign off on each procedure step. The results were then regularly entered into the database, including all measurements, such as leakage current. Statistics were kept on wire bonding failures, defective strips, and so forth.

Exhaustive testing was done on each item before integration with a larger assembly. Some examples already discussed are chip testing,

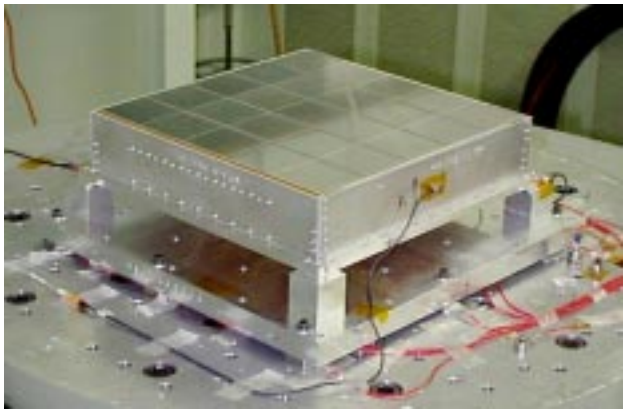

Figure 3.1.10. Photograph of the first instrumented prototype tray mounted on the shake table at GSFC.

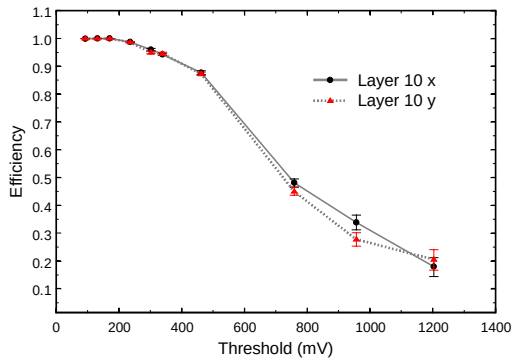

Figure 3.1.11. The efficiency in Layer 10 versus threshold, measured during the beam test from single electron tracks at normal incidence. The efficiency for each of the first three threshold values is greater than 99.9% for both the *x* and *y* layers. Inefficiency due to dead areas between detectors is not included. The nominal threshold for beam-test running was 170 mV (which is what was used for the noise measurement in Figure 3.1.2).

hybrid testing, and ladder testing. The finished trays were also tested by connecting them one-at-a-time into the DAQ interface and also by stacking them 8-at-a-time (while still in their protective boxes) into a cosmic-ray telescope.

In several cases time-consuming repairs were needed on ladders and hybrids (such as replacing a chip on a hybrid). Also, as noted in Section 3.1.10, the bias connection appears to have failed in two ladders after mounting to the tray. Those problem areas are under study in order to improve procedures to minimize the need for repairs in construction of the LAT flight instrument.

3.1.9 BTEM Tracker Assembly

Assembly of the tracker module included mounting of the bottom tray on the base plate, stacking of the remaining trays, attachment of the 8 readout cables, mounting of the walls, and threading and tensioning of the Vectran cables through the corner posts. In addition, a repeater board was attached to the end of each Kapton cable, and 8 twist-pair cables were routed from the repeater cards to the remote VME crate. The completed module is shown in Figure 3.1.12.

The walls are 1.5 mm thick aluminum (carbon-fiber will be used in the LAT flight instrument). They serve to hold the stack together and greatly stiffen the structure. They also serve as the heat path for cooling, provide EMI shielding, and shield the detectors from light.

Stacking of the trays proceeded smoothly and quickly, with no problems fitting parts together. Reducing the parts count in the spacers and pins between tray corner posts can save time in the future. Most of the Nanonics connectors on the Kapton cables attached easily, but in a few cases the tray structure interfered, requiring the circuit board to be loosened and pulled away slightly while inserting the connector. Additional clearance will be designed into the next iteration. There was no difficulty

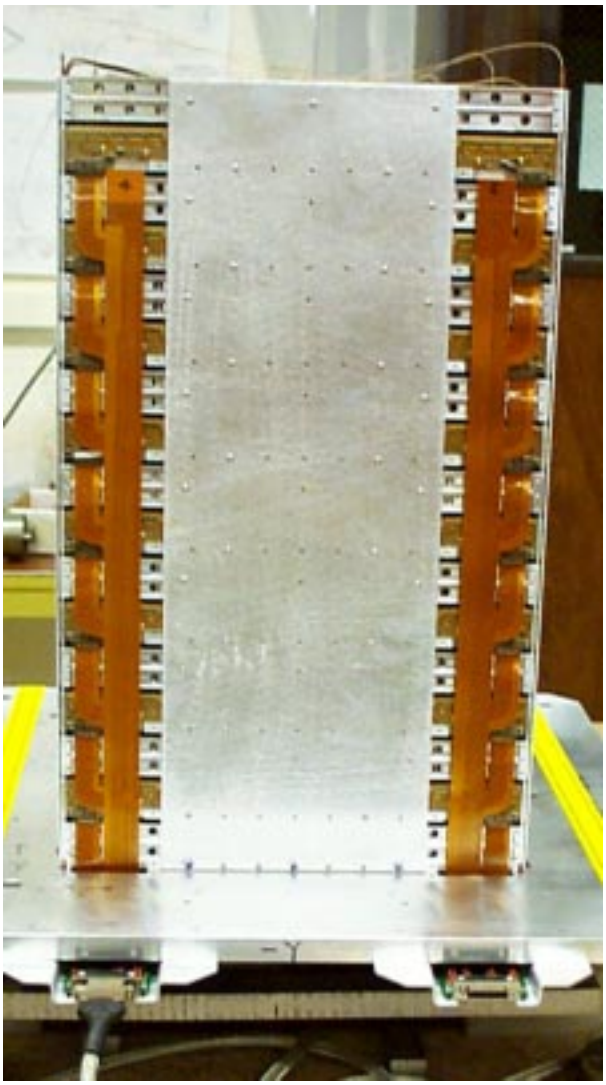

Figure 3.1.12. The BTEM tracker with side panels removed to expose two of the readout cables. Two repeater cards are visible at the bottom, with one connected to a Glenair cable.

attaching the walls and threading the Vectran cables. However, further studies need to be made of the Vectran cable termination procedures, as we were unable to obtain the desired tension of 220 Newtons (whether these cables are necessary at all will be reviewed).

3.1.10 BTEM Tracker Test Results

Initial testing of the Tracker concentrated on verifying the functionality and performance of the detectors and the electronics. This was accomplished first with noise-occupancy scans and with cosmic rays, as illustrated in Figure 3.1.3 and Figure 3.1.2. More extensive tests are in progress, making use of the beam-test data. For example, Figure 3.1.11 shows a measurement of the dependence of the efficiency on the threshold. These results demonstrate that essentially 100% efficiency is obtained within the detector fiducial volume while still satisfying the noise occupancy requirements. Note that the 50% efficiency point on the curves is at about 750 mV threshold, which should correspond to the average signal of a MIP (about 5.3 fC). This indicates an amplifier gain of about 140 mV/fC, which is in accord with the design goal.

Similar results are obtained in all but three of the detector ladders. One ladder is uniformly noisy (with a noise occupancy of about 10^{-3}) but still fully efficient at the nominal threshold. Therefore, it was operated in the beam test with a 340 mV threshold, which gives an efficiency for that ladder of about 94%. The reason for this excess noise will be investigated in the lab after the conclusion of the beam test.

One full ladder and a single detector of another ladder have very low efficiency and appear to be only slightly biased. After the conclusion of the beam test we will investigate why the bias connection was not made or was broken and then design assembly and QC procedures that will avoid this problem in the future.

Of the 41,600 individual channels that are connected to detector strips, outside of the one noisy ladder only a handful show excess noise. The number of noisy channels was low enough that it was not necessary to mask any from the readout or trigger during the beam test, including the self-triggered running. In summary, 98.5% of the 130 ladders in the BTEM are fully functional, while 97.7% exceed simultaneously the GLAST noise-occupancy and efficiency requirements.

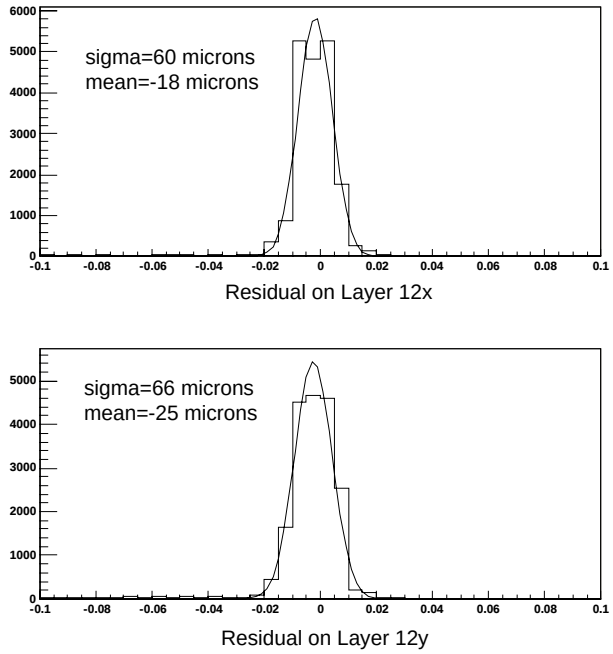

Figure 3.1.13. Tracker hit residuals in Layer 12, measured with respect to 10 GeV electron tracks defined in the 6 layers surrounding Layer 12. No alignment corrections have been made.

The Tracker resolution has also been studied using high-energy electrons from the test beam. The rms single-hit resolution is expected to be just the strip pitch divided by $\sqrt{12}$, which is 56 microns for the BTEM. The resolution is measured by finding and fitting tracks in one set of layers and then measuring the residual in a separate layer. Figure 3.1.13 shows the result of one such analysis, using 10 GeV electrons. Assuming negligible multiple scattering, so that the straight-line track fit is valid, the width of the observed distribution should, and does, closely reflect the expected resolution. In this analysis no alignment corrections have been applied in the reconstruction and analysis. The small deviations from zero of the means of the residual distributions indicate that misalignments are small compared with the intrinsic resolution.

Table 3.1.2. Milestones for the GLAST Tracker technology optimization.

Propose Date	Item	Milestone	Actual Date
6/1/98	Start Program		7/1/98
7/15/98	Silicon Detectors: select redundancy scheme.	Final silicon-strip detector design completed.	8/1/98
12/1/98	Silicon detectors from 6" wafers delivered.		1/15/99
2/1/99	Design Review on precision assembly.	Validation of the production alignment methods.	not yet reviewed
2/1/99	Design Review on advanced tower design.	Thermal/structural design completed.	not yet reviewed
9/15/99	Fabrication of front-end electronics ASICs in new process begins.		9/1/99
12/1/99	Optimized silicon detectors from 6" wafers received.	Validation of the final detector design.	8/1/99

Similar results are obtained for the other *x,y* planes. Figure 3.1.14 shows the distributions of the means of the residual distributions for all but the lowest 3 layers in the *x* and *y* projections. The width of this distribution indicates the quality of the Tracker mechanical assembly and is well within specifications.

3.1.11 Milestones and Conclusions

With the exception of three formal design reviews, all Tracker milestones proposed up through Option-1 were achieved. Table 3.1.3 lists the milestones connected with the BTEM Tracker construction. A very successful EMI protection scheme was implemented in the BTEM Tracker but was not formally reviewed. The corresponding scheme for the flight version will be reviewed in 2000 in the context of an overall review of the Tracker readout electronics. Otherwise, all milestones were achieved by the scheduled ending date, although complete analysis of the beam-test data will be an ongoing endeavor throughout 2000.

Table 3.1.2 lists the milestones concerning Tracker development work that goes beyond the BTEM. Review of the precision assembly is on hold pending further analysis of the results obtained with the BTEM, and the advanced tower design (all carbon-composite), while in progress, is not quite ready for a formal review. On the other hand, the detector design is well in hand, with the final mask design needing only a final specification of the size and strip pitch. The front-end electronics are in the process of being redesigned for the 0.5 μm HP process, and a prototype of the amplifier-discriminator section has already been fabricated and tested in that process. The final design will take place after a thorough review of number of desired design modifications.

In conclusion, the BTEM Tracker module was completed and is operating very successfully and within specifications in the SLAC test beam. A great deal was learned from the experience that is already leading to improved optimization of the design and major improvements in the assembly procedures and quality control.

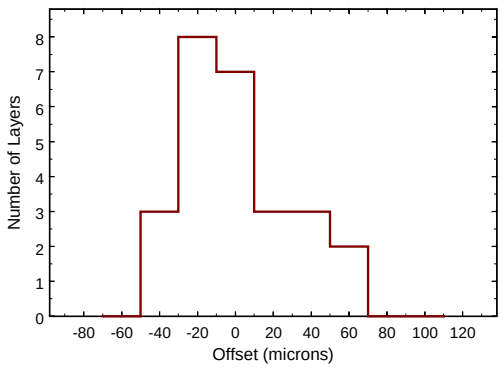

Figure 3.1.14. Distribution of the measured offset of Tracker layers with respect to the surrounding layers. The measurement was made using electron tracks from the beam-test data.

Table 3.1.3. Milestones for the BTEM Tracker up through January 2000.

Proposed Date	Item	MILESTONES	Actual Date
6/1/98	Start Program.		7/1/98
7/1/98	Prototype FEE ASIC's tested.	Validation of the functionality of the front-end electronics	8/1/98
7/1/98	Silicon Detectors tested.	Validation of the detector design and QA methods.	8/1/98
9/1/98	Full length ladder plus electronics tested.	Front-end electronics design validated.	9/1/98
10/15/98	Prototype tray assembly complete; tray design review.	Tray design and fabrication methods validated.	1/15/99
11/1/98	First production tray assembled	Tray production validated	9/2/99
3/15/99	Last tray complete. Begin prototype tracker assembly.	Validation of the tray assembly QC procedures	10/25/99
5/1/99	Review of tower EMI suppression design		not reviewed
5/15/99	Prototype Tracker assembly complete		11/15/99
7/15/99	Cosmic Ray test of prototype tracker complete		11/26/99
8/15/99	GLAST tower prototype assembly complete	Validation of the integrated mechanical design and the mechani-cal/electrical/thermal interfaces	12/1/99
9/1/99	GLAST Tower Prototype Beam Test begins		12/1/99
12/31/99	GLAST Tower Prototype Beam Test complete	Validation of the tower prototype from beam-test results, compared with Monte Carlo model.	1/31/00 (analysis in progress)

3.1.12 References

W.B. Atwood *et al.*, "Beam Test of Gamma-Ray Large Area Space Telescope Components," Nucl. Instr. Meth. A, in press, SLAC PUB 8166 (1999).

J.A. Hernando *et al.*, "The Silicon Tracker/Converter for the Gamma-Ray Large-Area Space Telescope," Nucl. Instr. Meth. A 435 (1999) 224.

R.P. Johnson *et al.*, "An Amplifier-Discriminator Chip for the GLAST Silicon-Strip Tracker," IEEE Trans. Nucl. Sci. 45 (1998) 927.